National Conference with International Participation
ENGINEERING MECHANICS 2006
Svratka, Czech Republic, May 15 – 18, 2006

paper no.
119

WHIRL FLUTTER ANALYSIS OF THE COMMUTER AIRCRAFT AEROELASTIC MODEL WING – ENGINE COMPONENT

J.Čečrdle *

Summary: *The submitted paper deals with whirl flutter of turboprop aircraft. It gives a summary of the airworthiness regulations requirements and the theoretical background concerning the mentioned aeroelastic phenomenon. The whirl flutter analysis was performed by means of the NASTRAN program system supported by other specialized software packages. The analysis was made on an aeroelastic model of the wing – engine component of a commuter aircraft for 40 passengers.*

1. Introduction

Whirl flutter is a dynamic aeroelastic phenomenon, which may occur on the turboprop engine powered aircraft, especially twin or four-engine co[...]e wing. Rotating parts like propeller or turbine increase the number of structural degrees of freedom and cause additional forces and moments (centrifugal, gyroscopic). Moreover during flight the rotating propeller causes a complicated flow field and interference effects between wing, nacelle and propeller. The whirl flutter phenomenon grounds upon the asymmetric distribution of the pull force on the transversely vibrating propeller.

Fig.1 – Lockheed L188 Electra II

Whirl flutter may cause the propeller mounting unstable vibrations, even failure of the engine, nacelle or whole wing. Among the most grievous events of the whirl flutter are two catastrophic crashes of the Lockheed L188 Electra II (4-engine turboprop aircraft for 100 passengers - fig.1) in 1959, when engines got broken off during the flight.

2. Airworthiness Regulation Requirements

Airworthiness regulations requirements to certify the whirl flutter stability were limited to the twin or four engine aircraft in the past. Currently the demands have been extended also to one engine configuration, despite that it is not as critical as the former one.

The regulation FAR 23 (Normal, Utility and Aerobatic Airplanes) requires in the §23.629(e)(1)(2) taking into account the influence of the rotational degrees of freedom of the propeller plane and significant elastic, inertia and aerodynamic forces. Also the changes in the stiffness and damping of the propeller – engine – nacelle – structure system must be considered.

* Ing. Jiří Čečrdle, Ph.D.: Aeronautical Research and Test Institute (VZLU); Beranových 130; 199 05 Praha – Letňany; tel.:(+420) 225 115 123; fax:(+420) 283 920 018; e-mail: cecrdle@vzlu.cz

The regulation FAR 25 (Transport Airplanes) moreover requires in the §25.629(d)(4)(i)-(iv) the failure states to be included. Specifically failure of any single element supporting any engine (engine bed beams), any single engine failure which would reduce the yaw or pitch rigidity of the rotational axis, absence of the propeller aerodynamic forces from the feathering of any single propeller or critical combination of two propellers for four and more engine aircraft, in addition any single feathered propeller must be paired with above mentioned failures and finally any single propeller rotating with the highest probability of overspeeding.

The MIL-A-8870(AS) military standard includes in addition in the §3.2.1.3.1 the battle damage. There is a general notice about prevention of the whirl flutter in the §3.2.1.7. Finally the §4.2.1.1.10 specifies the whirl flutter analysis procedure; particularly it demands to perform an analysis for complete propeller – engine plus the airplane model.

3. Theoretical Background

Engine flexible mounting is represented by two rotational springs (stiffness K_Ψ, K_Θ) as illustrated in fig.2. Propeller is considered as rigid, rotating with angular velocity Ω. System is in the airflow of velocity V_∞.

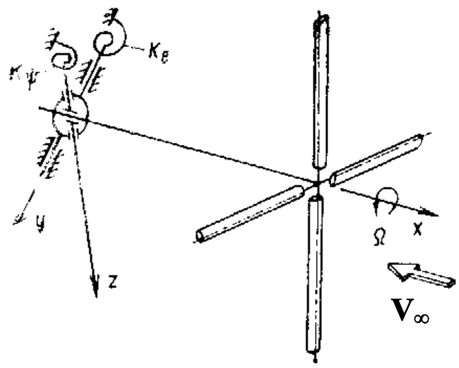

Fig.2 – Gyroscopic system with propeller

Neglecting propeller rotation and the aerodynamic forces, the two independent mode shapes (yaw – around vertical axis, pitch – around lateral axis) will emerge (fig.3) with angular frequencies ω_Ψ and ω_Θ.

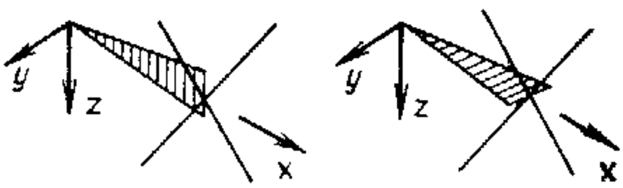

Fig.3 – Independent mode shapes

Considering the propeller rotation, the system changes to the characteristic gyroscopic motion. The gyroscopic effect makes two independent mode shapes merge to rotational motion (fig.4). The propeller axis makes an elliptical movement. The orientation of the propeller axis movement is backward relatively to the propeller rotation for the mode with lower frequency (backward whirl mode – fig.4a) and forward relatively to the propeller rotation for the mode with higher frequency (forward whirl mode – fig.4b). It corresponds to the low-speed and high-speed precession of the gyroscopic system. The mode shapes of mentioned gyroscopic modes are complex, since independent yaw and pitch modes have a phase shift 90°. Condition of real mode shapes corresponds to the state with no total damping of the system.

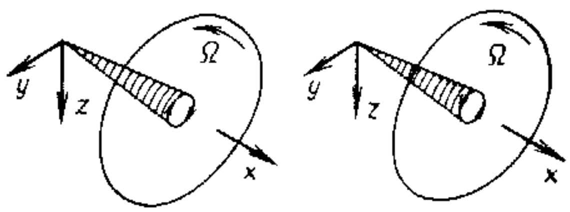

Fig.4ab – Backward and forward whirl mode

The described gyroscopic mode shapes make harmonic changes of propeller blades angles of attack. They give rise to non-stationary aerodynamic forces, which may under the specific conditions induce a flutter. Possible states

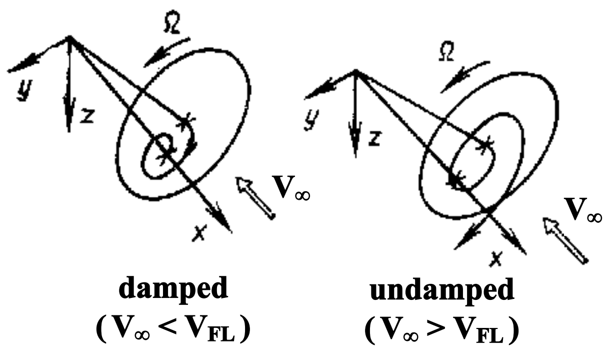

Obr.5ab - Stable and unstable state of gyroscopic vibrations for backward flutter mode

of the gyroscopic system from the flutter stability point of view for backward mode are explained in fig.5ab. Provided that the air velocity is lower than critical value ($V_\infty < V_{FL}$), the system is stable and the motion is damped. If the airspeed exceeds the critical value ($V_\infty > V_{FL}$), the system becomes unstable and motion is diverging. The limit state ($V_\infty = V_{FL}$) with no total damping is called critical flutter state and V_{FL} is called critical flutter speed.

The basic problem of analytical solution grounds on determination of the aerodynamic forces caused by the gyroscopic motion for the specific propeller blades. Considering no sideslip angle, the basic characteristics of aerodynamic forces can be obtained using quasi-steady theory (Forsching, 1984).

The equations of motion were set up for system described in fig.2 by means of the Lagrange approach. The kinematical scheme including gyroscopic effects is shown in fig.6. The independent generalized coordinates are three angles (φ, Θ, Ψ). Ranges for the angle Θ are $<z; Z>$ and $<x;X>$, for angle Ψ are $<\tilde{x}; X>$ and $<y; Y>$. We assume the propeller angular velocity constant ($\varphi = \Omega t$), mass distribution symmetric around X-axis and mass moments of inertia $J_Z \neq J_Y$. We will use a coordinate system X, Y, Z linked to the system.

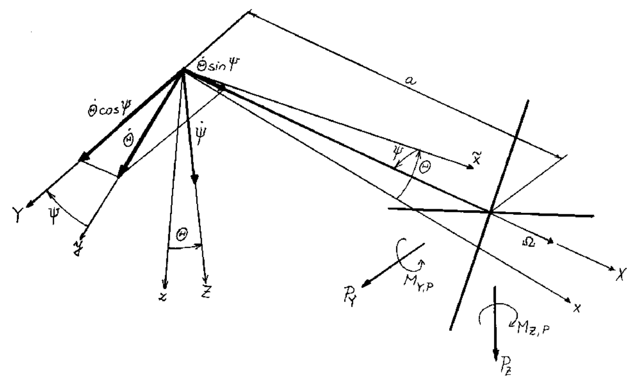

Fig.6 – Kinematical scheme of the gyroscopic system

Then kinetic energy is:

$$E_K = \frac{1}{2} J_X \Omega^2 + J_X \Omega \Psi \dot{\Theta} + \frac{1}{2} J_Y \left(\dot{\Theta}^2 + \dot{\Psi}^2 \right) \tag{1}$$

Potential energy is:

$$U = \frac{1}{2} K_\Theta \Theta^2 + \frac{1}{2} K_\Psi \Psi^2 \tag{2}$$

Description of the structural damping is:

$$D = \frac{1}{2} \frac{K_\Theta \gamma_\Theta}{\omega} \dot{\Theta}^2 + \frac{1}{2} \frac{K_\Psi \gamma_\Psi}{\omega} \dot{\Psi}^2 \tag{3}$$

Then equations of motion become:

$$\begin{aligned} J_Y \ddot{\Theta} + \frac{K_\Theta \gamma_\Theta}{\omega} \dot{\Theta} + J_X \Omega \dot{\Psi} + K_\Theta \Theta &= M_{Y,P} - a.P_Z \\ J_Y \ddot{\Psi} + \frac{K_\Psi \gamma_\Psi}{\omega} \dot{\Psi} - J_X \Omega \dot{\Theta} + K_\Psi \Psi &= M_{Z,P} + a.P_y \end{aligned} \tag{4}$$

We formulate the propeller aerodynamic forces by means of the aerodynamic derivatives (Ribner, 1945) and make the simplification for the harmonic motion, then the final whirl flutter matrix equation will become:

$$\left(-\omega^2[M]+j\omega\left([D]+[G]+q_\infty F_P\frac{D_P^2}{V_\infty}[D^A]\right)+\left([K]+q_\infty F_P D_P[K^A]\right)\right)\times\begin{bmatrix}\overline{\Theta}\\ \overline{\Psi}\end{bmatrix}=\{0\} \tag{5}$$

The limit state emerges for the specific combination of parameters V_∞ and Ω, when angular velocity ω is real. The whirl flutter characteristics are explained in fig.7, which describes influence of the propeller relative velocity (V_∞ / (ΩR)) to the stability of undamped gyroscopic system. Increasing the propeller relative velocity makes increasing of the necessary stiffnesses K_Θ , K_Ψ. Influence of the structural damping and also influence of distance propeller – mode shape node is described in fig.8.

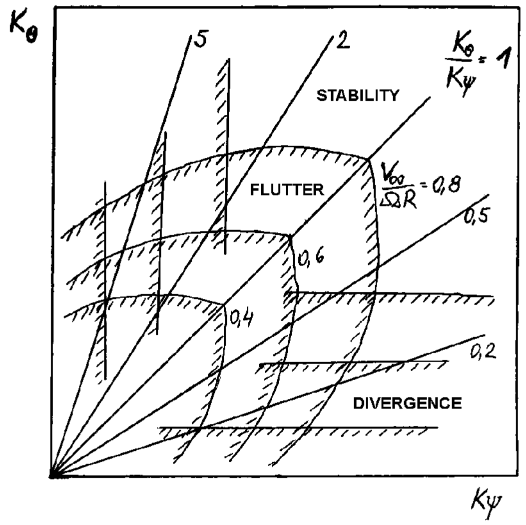

Fig.7 – Influence of the propeller relative velocity (V_∞/ (ΩR)) to the stability of undamped gyroscopic system

Globally said, the whirl flutter appears at the gyroscopic rotational vibrations, the flutter frequency is the same as the frequency of the backward gyroscopic mode. The critical state may be reached either due to increasing the air velocity or the propeller revolutions. Structural damping is a significant stabilization factor. On the contrary, the propeller pull force influence is barely noticeable. The most critical state is K_Θ = K_Ψ, it means ω_Θ = ω_Ψ when the interaction of both independent motions is maximal. A special case of the eq.(5) for ω=0 is the gyroscopic static divergence. The critical dynamic pressure for divergence is obtained from determinant:

$$\left|[K]+q_{DIV}F_P D_P[K^A]\right|=0 \tag{6}$$

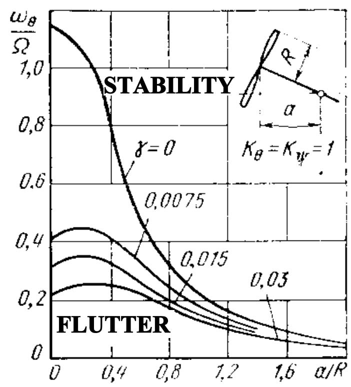

Fig.8 – Structural damping and propeller – mode shape node distance influences to the whirl flutter

4. Whirl flutter analysis procedure

Whirl flutter solution by means of the NASTRAN program system grounds on the Strip Aerodynamic Theory for the propeller at the windmilling mode. Propeller is assumed rigid. For the rest structure is used Wing – Body Interference Aerodynamic Theory (Giesing, J.P. – Kalman, T.P. – Rodden, W.P., 1972). For the flutter stability solution is used PK method. NASTRAN whirl flutter DMAP procedure is supplemented by the external preprocessor (program propf.for) for calculation of the propeller aerodynamic matrices (formally damping and stiffness matrices) and optionally for calculation of the down / side wash effects. The output data processing is possible by means of the whirl flutter option of the nasflat postprocessor program.

The analysis procedure is summarized in fig.9. The FE model can be prepared similarly as for the ordinary flutter analysis; model must include the grid at the propeller center of gravity with propeller mass characteristics. Aerodynamic model must be prepared for Wing – Body Interference Theory. Data for calculation of downwash and sidewash angles may be specified by means of the partitioning matrices (PARTNx). The first NASTRAN run calculates the down / side wash angles only. These data and other data concerning engine and propeller (propeller revolutions, inertia data, geometry, velocities, air characteristics etc.) are input to the external preprocessor (program propf.for) which calculates the propeller aerodynamic matrices and possibly down / side wash effects. These data are added to the NASTRAN input, formally as direct input to the stiffness and damping matrices. Partitioning matrices must be removed. The second NASTRAN run is the final one and makes a flutter stability calculation. The output data arrangement is different in comparison with ordinary flutter analysis, therefore the postprocessor (program nasflat) is recommended to use for calculation of the flutter state parameters and draw diagrams.

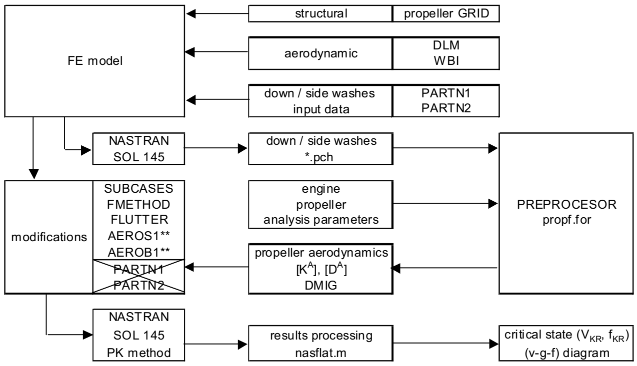

Fig.9 – Whirl flutter analysis procedure

The propeller aerodynamic forces and moments are calculated by eq.(7):

$$
\begin{aligned}
P_Y &= q_\infty F_p\left(c_{y\Psi}\Psi^* + c_{y\Theta}\Theta^* + c_{yq}\frac{\dot{\Theta}^* R}{V_\infty}\right)\ ;\ P_Z = q_\infty F_p\left(c_{z\Theta}\Theta^* + c_{z\Psi}\Psi^* + c_{zr}\frac{\dot{\Psi}^* R}{V_\infty}\right)\\
M_{Y,P} &= q_\infty F_P D_P\left(c_{m\Psi}\Psi^* + c_{mq}\frac{\dot{\Theta}^* R}{V_\infty}\right)\ ;\ M_{Z,P} = q_\infty F_P D_P\left(c_{n\Theta}\Theta^* + c_{nr}\frac{\dot{\Psi}^* R}{V_\infty}\right)
\end{aligned}
\tag{7}
$$

Effective angles are determined by Eq.(8), aerodynamic derivatives are given from propeller blade integrals (Rodden, W.P., Rose, T.L., 1989).

An option to include the downwash and sidewash effects may be important for configuration with engines mounted to the wing. Downwash and sidewash angles behind the propeller describe interference between propeller and nacelle. Induced downwash (at the vertical plane) and sidewash (at the horizontal plane) angles are added to the effective static angles (fig.10) by the eq.(8):

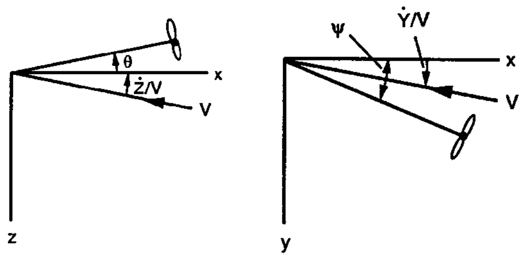

Fig.10ab – Effective static downwash and sidewash angles

$$
\Theta^* = \Theta + \frac{\dot{z}}{V} - \frac{w_1}{V}\ ;\Psi^* = \Psi - \frac{\dot{y}}{V} + \frac{w_2}{V} \tag{8}
$$

Above mentioned induced down / side wash angles dependent on the reduced frequency can be obtained from the lift solution by partitioning the interference coefficients. Downwash effects can be calculated either in vertical plane (downwash only) or in both vertical and horizontal planes (downwash and sidewash). The former choice assumes the nacelle modeled as Z body (vertical forces only), the latter one as ZY body (both vertical and lateral forces). Downwash effect influences only the aerodynamic stiffness matrix; influence to the aerodynamic damping matrix is neglected. Only interference between propeller and nacelle is included, interference between propeller and wing is neglected.

5. Whirl flutter analysis of the Ae 270 aircraft

Fig.11 – Ae 270 aircraft

The first specific task regarding the whirl flutter is calculation of the Ae 270 aircraft (Cecrdle, 2001, 2002). The Ae 270 aircraft is a 10 seat small transport aircraft powered by single nose mounted turboprop engine (fig.11). Since the engine is mounted to the relatively stiff fuselage, the analysis was performed on the propeller – engine – engine bed system (fig.12a). Model includes engine, propeller and engine bed inertia characteristics and engine bed and engine mount-isolators stiffness characteristics. Two engine vibration modes (vertical, lateral – fig.12bc) were included to the analysis, downwash effects were neglected.

Modal characteristics (natural frequencies, node points) of mentioned modes were tuned using data from ground vibration tests. The results summary is shown in the fig.13, it describes the influence of the vertical and lateral engine vibration mode to the whirl flutter characteristics. Flutter, divergence and stability areas well correspond to the theory (fig.7).

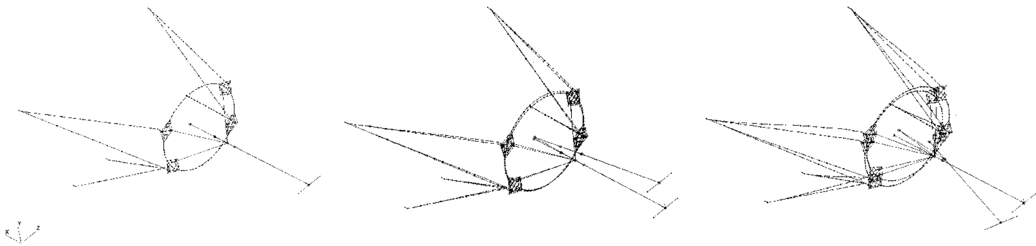

Fig.12abc – Ae 270 whirl flutter analysis (model, engine vertical and lateral bending modes)

Possibilities from the stability point of view (stability, flutter, divergence) are documented in the fig.14 – 16 (v-g-f diagrams). The nominal state of the Ae 270 engine installation is in the stable area with sufficient reserve.

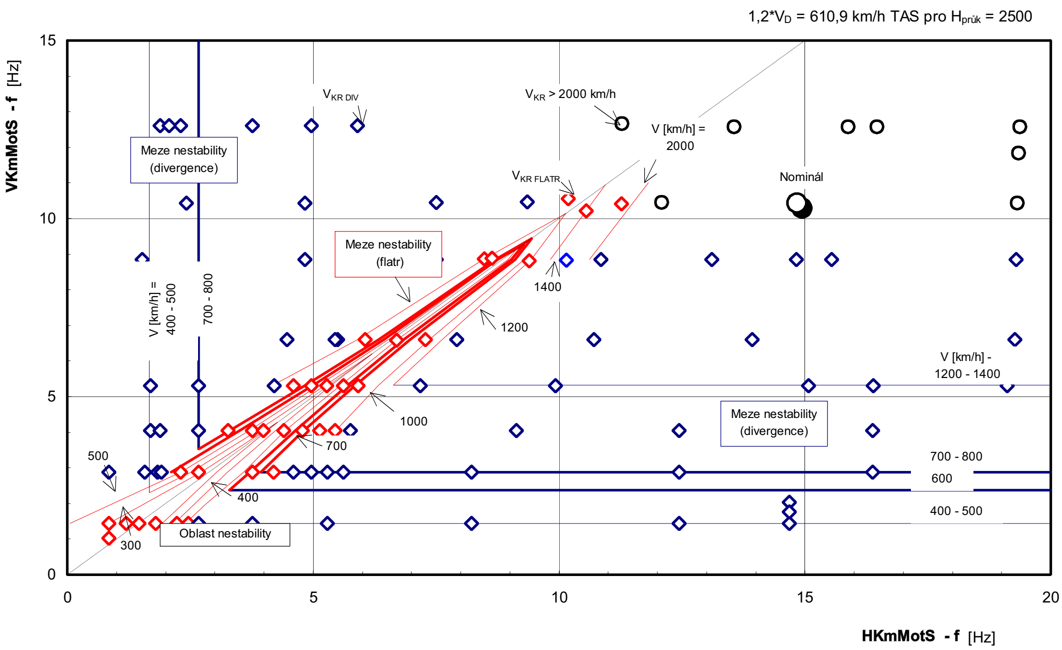

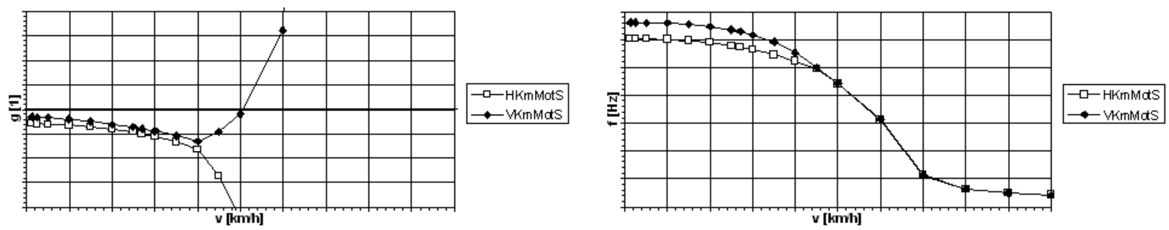

Fig.15ab – V-g-f diagram – flutter case

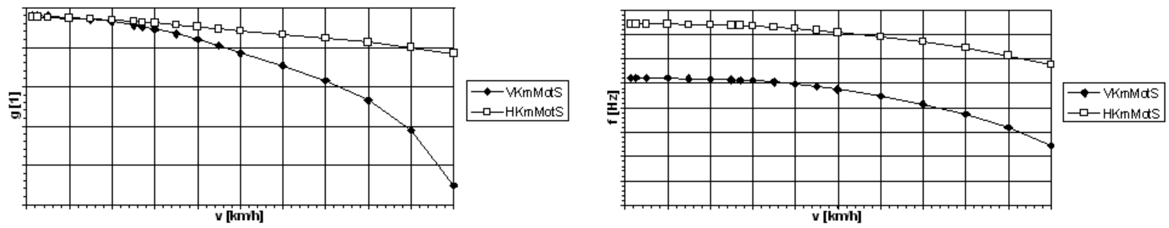

Fig.14ab – V-g-f diagram – stability case

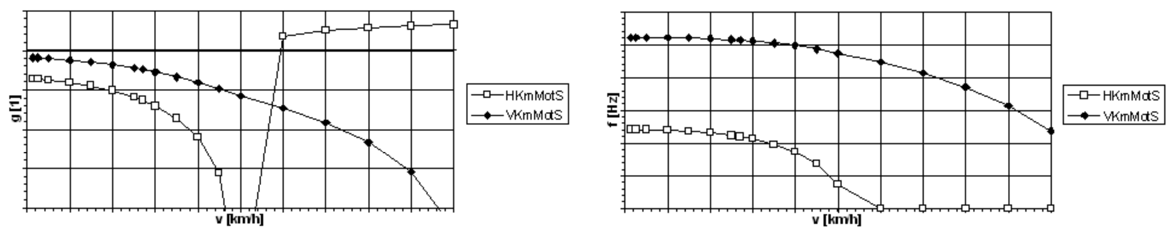

Fig.16ab – V-g-f diagram – divergence case

6. Whirl flutter analysis of the L 610 aircraft aeroelastic model

Fig.17 – L-610 aircraft

The task regarding the whirl flutter this paper is focused on is the calculation of the L 610 aircraft aeroelastic model (Cecrdle, 2005). The L 610 aircraft is a 42 seat twin turboprop engine transport aircraft (fig.17). The aeroelastic model of the L 610 (length scale 1/5; velocity scale 1/6) was developed and manufactured at the VZLU for wind tunnel flutter tests (Malecek, 1990). Now the hardware model, database of the structural parameters and stiffness, modal and wind tunnel flutter test results are used for research projects.

Calculation of the whirl flutter was performed on the model of the wing – engine system. Contrary to the former example, this task includes the down / side wash effects and dynamic characteristics of the wing.

The wing / engine hardware model (fig.18) consists of a beam placed at the wing elastic axis, paper / balsa coachwork and concentrated lead weights. The aileron is the similar structure as the wing, the aileron drive stiffness is modeled via metal spring, and also a hydraulic actuation is possible. The engine mounting is modeled via two rotational springs (engine bed) and two translational springs (engine mount-isolators).

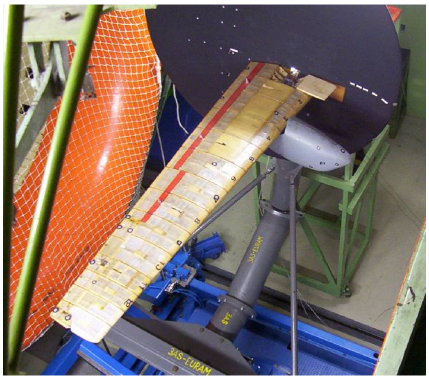

Fig.18 – L-610 aircraft wing / engine aeroelastic model

The FE model was prepared using the hardware model structural data. It corresponds to the described hardware model structure. (elements BAR, CONM2, CELAS, conditions RBE2, MPC). Model is either fixed at the wing root or the antisymmetric support, allowing the rolling to be specified (CELAS). The model also allows the selection of the fuel tank filling and the aileron balancing by the appropriate mass set selection. Changes in the aileron drive and engine mounting stiffness are also possible. The structural part of the model is shown in fig.19.

The aerodynamic model is prepared for the Wing – Body Interference Aerodynamic Theory. The wing and spliter (to prevent the induced effects at the wing root) are modeled as Doublett – Lattice macroelements (CAERO1), the nacelle is modeled as the Slender and Interference Body (CAERO2). Structural and aerodynamic parts are connected by means of the beam splines, spliter is grounded via surface spline. The aerodynamic part of the model is shown in fig.20.

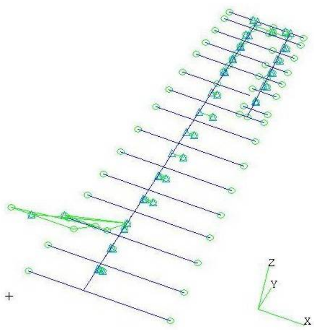

Fig.19 – Structural FE model

Model was verified using results of the modal tests and wind tunnel flutter tests. Experimental modal characteristics and aileron flutter characteristics were compared with corresponding analytical results. The analysis and experimental results agreement have been found on the acceptable level.

Before performing the whirl flutter calculations, the engine / propeller data were modified in accordance with demands on the programs used. For this purpose, the data of Walter M 602 engine and Avia V 518 propeller were used. The original data were scaled down according appropriate model scale factors. At first, the calculation of cantilevered engine with mount-isolators and engine bed with 4 degrees of freedom were performed to obtain the flutter and divergence areas. The results are similar to those already shown in fig.13. Then was selected the suitable configuration of engine mounting stiffness to find the whirl flutter for the next steps.

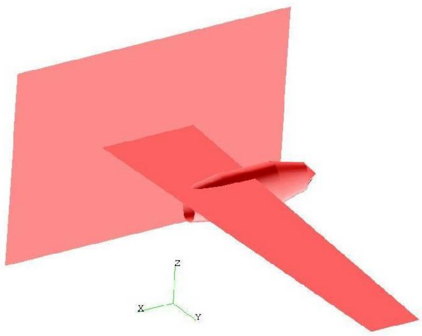

Fig.20 – Aerodynamic FE model

The modal analysis was performed by means of the Lanczos method; the results summary is listed in tab.1.

All the flutter calculations were performed by means of the PK method; zero Mach number and air density of ISA value for the sea level. The wing middle aerodynamic chord was used as the reference chord for the reduced frequency calculation. Calculations were performed for air velocities up to 80 m.s^{-1}. A maximum combination of the mode shapes corresponds to the tab.1; also suitable mode shape subsets were used to determine critical combinations for a specific flutter instability types.

Tab.1 – Modal characteristics summary

#	Mode shape title	Abbr.	f_0 [Hz]
1	1st engine vertical vibrations	1.EVVib	1.327
2	1st engine horizontal vibrations	1.EHVib	1.462
3	Rolling on suspension	Rol	2.034
4	1st wing vertical bending	1.WVB	6.423
5	1st wing horizontal bending	1.WHB	8.209
6	Aileron flapping (rotation)	AileRot	13.323
7	1st wing torsion	1.WT	14.656
8	2nd wing vertical bending	2.WVB	17.886
9	2nd wing horizontal bending	2.WHB	22.309
10	2nd wing torsion	2.WT	24.607

The last preparatory step was the calculation of the ordinary flutter with no gyroscopic effect. The results of this analysis were used as the comparative set to be able to determine the influence of the gyroscopic effect. The two types of flutter instability were found. The first one is the bending – torsion – aileron flutter on the antisymmetric suspension for the critical combination of 4 modes (# 3, 6, 7, 8). The minimal

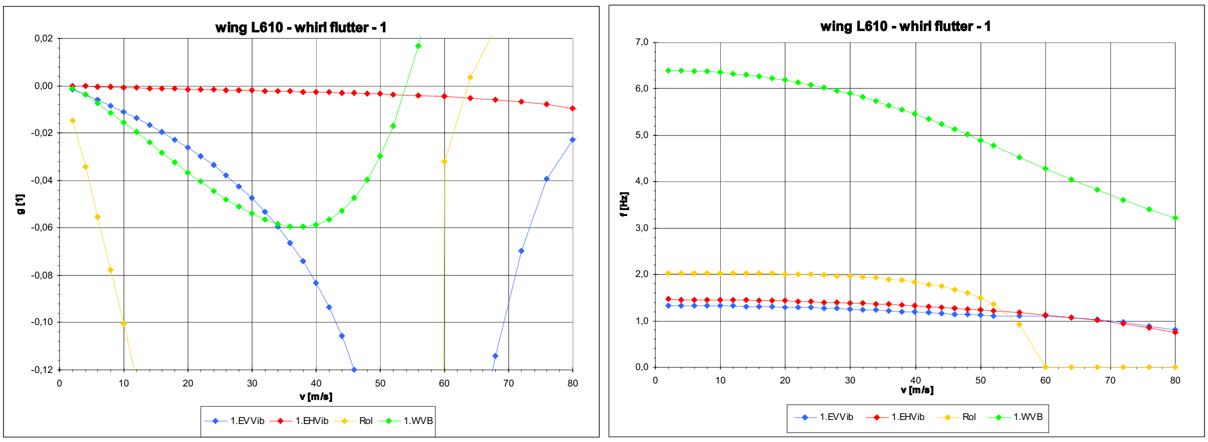

Fig.22ab – v-g-f diagram – Wing bending flutter (4 DOFs)

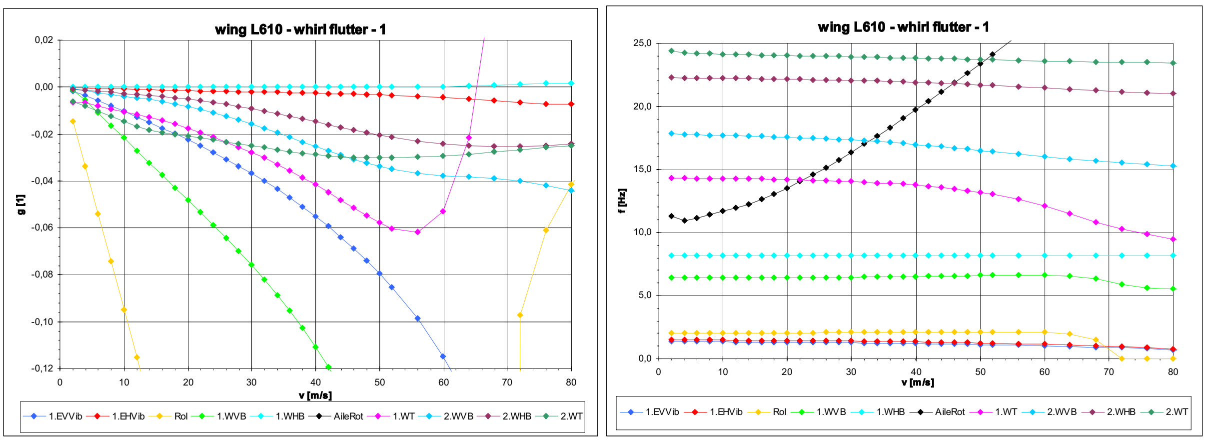

Fig.21ab – v-g-f diagram - Aileron flutter (10 DOFs)

Tab.2 – Whirl flutter analyses summary

Mode selection	Critical state	No downwash	Downwash	Down + side wash	Influence – downwash
1, 2, 3, 4, 5, 6, 7, 8, 9, 10	V_{FL} [m.s^{-1}]	36.81	37.94	37.95	+3.07 %
	f_{FL} [Hz]	0.7	0.7	0.7	
1, 2, 3, 4, 5, 6, 7, 8, 9	V_{FL} [m.s^{-1}]	36.63	37.64	37.64	+2.76 %
	f_{FL} [Hz]	0.7	0.7	0.7	
1, 2, 3, 4, 5, 6, 7, 8	V_{FL} [m.s^{-1}]	36.54	37.48	37.49	+2.57 %
	f_{FL} [Hz]	0.7	0.7	0.7	
1, 2, 3, 4, 5, 6, 7	V_{FL} [m.s^{-1}]	36.38	37.20	37.21	+2.25 %
	f_{FL} [Hz]	0.8	0.8	0.8	
1, 2, 3, 4, 5, 6	V_{FL} [m.s^{-1}]	36.38	37.17	37.18	+2.17 %
	f_{FL} [Hz]	0.9	0.8	0.8	
1, 2, 3, 4, 5	V_{FL} [m.s^{-1}]	37.10	37.30	37.30	+0.53 %
	f_{FL} [Hz]	0.9	0.9	0.9	
1, 2, 3, 4	V_{FL} [m.s^{-1}]	37.10	37.30	37.30	+0.54 %
	f_{FL} [Hz]	0.9	0.9	0.9	
1, 2, 3	V_{FL} [m.s^{-1}]	36.84	37.02	37.02	+0.48 %
	f_{FL} [Hz]	0.9	0.9	0.9	
1, 2	V_{FL} [m.s^{-1}]	42.95	43.07	43.07	+0.28 %
	f_{FL} [Hz]	0.4	0.4	0.4	

critical flutter speed was 65.2 m.s^{-1}; critical frequency was 11.3 Hz. This flutter type occurred also for higher degree of freedom combinations. For the combination of mode shapes up to #5 (without aileron flapping mode), the above mentioned instability type changes to the second one, the wing bending flutter on the antisymmetric suspension for the critical combination of 2 modes (#3, 4). The minimal critical flutter speed was 54.0 m.s^{-1}; critical frequency was 4.6 Hz. Also the divergence of the wing suspension were found for some combinations, the critical speed is obvious from the v-g-f diagrams. The results are in accordance with assumptions. There is no whirl flutter if the gyroscopic effect is neglected, and there occurs only aileron flutter or wing flutter. The results are shown in figs.21 and 22.

The final whirl flutter calculations were performed at the three steps: With no downwash effects, including downwash (vertical), including downwash and sidewash (horizontal). Apart from the above mentioned flutter instability types, the whirl flutter instability occurred for critical combination of two engine vibration modes (#1, 2). The values of whirl flutter speed

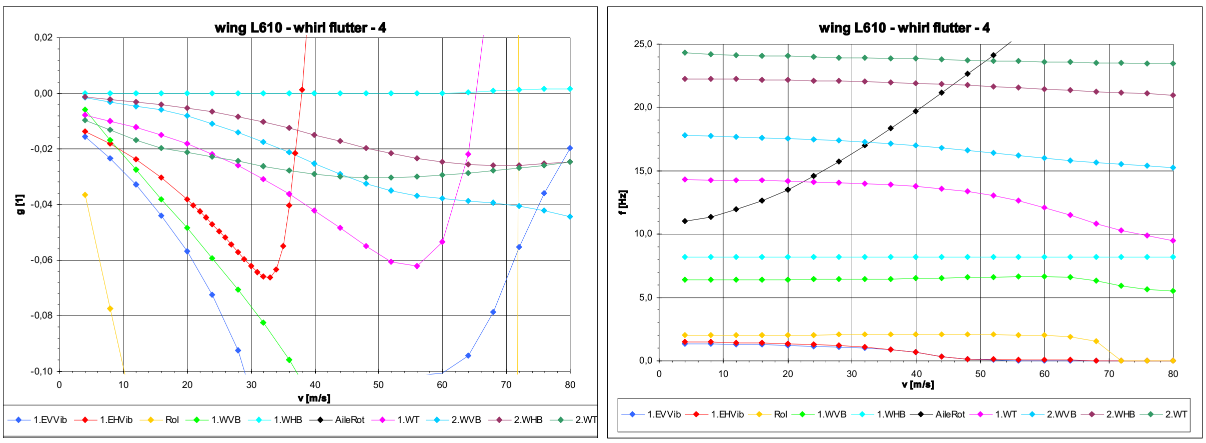

Fig.23ab – v-g-f diagram – Whirl flutter with downwash effect, also aileron flutter (10 DOFs)

Fig.24ab – v-g-f diagram – Whirl flutter with downwash effect, also bending flutter (4 DOFs)

for specific combinations of the mode shapes and separate analysis steps (down / side wash including) are summarized in tab.2. The influence of the gyroscopic effect to the other flutter types is not noticeable. The influence of the downwash effect is slightly stabilizing (see tab.2), the influence of the sidewash effect is barely noticeable. The results v-g-f diagrams are presented for the "downwash included" analyses set in figs.23 and 24. Presented diagrams represent the same mode selections, as presented in figs.21 and 22, and so there are whirl flutter instable root and either aileron or wing bending instable root.

7. Conclusion

The submitted paper deals with the aircraft structure whirl flutter problems. First part describes the theoretical aspects of mentioned aeroelastic phenomenon and the procedure of analysis by means of NASTRAN and other auxiliary program systems. Also airworthiness regulation requirements concerning the whirl flutter are summarized. Second, practical part documents the whirl flutter calculations. The Ae 270 aircraft calculation is outlined first.

The main emphasis is focused on the L-610 aeroelastic model analysis. Analyses were performed on the wing – engine model. Model was verified via modal test and wind tunnel flutter test (aileron flutter) data. The whirl flutter analyses were divided into several groups. First, a large parametric study on the cantilevered engine bed – engine mount-isolators – engine – propeller system was done. The parameters were engine vertical and horizontal vibrations natural frequency. The purpose of this phase was to find the whirl flutter area. In accordance with assumptions, the whirl flutter occurs when the vertical and horizontal vibrations frequency ratio is close to 1. The divergence occurs, when any frequency is decreased below a specific value.

Then the appropriate parameters of the model were set. The next phase was calculations on the wing – engine bed – engine mount-isolators – engine – propeller system model with no gyroscopic effect to obtain a comparative set of results and to get the other structural instability flutter types (aileron flutter, bending flutter). The final phase concerned whirl flutter calculations for several mode shape selections (from 2 to 10) with variations of downwash and sidewash effects. Depending on the mode shape selection, apart from the whirl flutter, also other specific types of instability occur; nevertheless the gyroscopic effect makes no influence on these other instabilities.

The calculations verified the necessity of the regulations demand to include the dynamic characteristic of the rest structure in the whirl flutter analysis. Influence of the downwash effect (in vertical plane) is slightly stabilizing. On the one hand including the downwash effect makes the analysis more accurate. On the other hand, neglecting it is on the side of safety. Influence of the sidewash effect (in the horizontal plane) is barely noticeable.

8. Acknowledgements

The paper was prepared in the frame of the project "Research on Strength of Low-weight Structures with Special Regard to Airplane Structures" funded from the Czech Ministry of Education, project number MSM 0001066903.

9. References

Ribner, H.S. (1945) Propellers in Yaw, NACA Report 820

Ribner, H.S. (1945) Formulas for Propellers in Yaw and charts of the Side – Force Derivatives, NACA Report 819

Houbolt, J.C. – Reed, W.H. (1962) Propeller – Nacelle Whirl Flutter, Journal Aerospace Sciences, Vol.29, 1962, pp.333 – 346

Giesing, J.P. – Kalman, T.P. – Rodden, W.P. (1972) Subsonic Steady and Oscillatory Aerodynamics for Multiple Interfering Wings and Bodies, Journal of Aircraft, Vol.9, pp.693-702

Rodden, W.P. – Bellinger, E.D. (1982) Aerodynamic Lag Functions, Divergence and the British Flutter Method, Journal of Aircraft, Vol.19, pp.596-598

Forsching, H.W. (1984) Grundlagen der Aeroelastik (translation: Osnovy Aerouprugosti), publ. Mašinostroenie Moscow, IB 3112

Rodden, W.P. – Rose, T.L. (1989) Propeller / Nacelle Whirl Flutter Addition to MSC/NASTRAN, Paper No.12, Proceedings of the 1989 MSC World User's Conference, Universal City, Ca.,U.S.A., March 1989

Maleček, J. (1990) Souhrnná zpráva o modelových experimentech pro ověření aeroelastické bezpečnosti L-610, VZLU Report, R-2583/90

Čečrdle, J. (2001) Výpočet vířivého flatru pomocí programového systému MSC.NASTRAN, National MSC.Software Users Conference, MSC.Software s.r.o., proceedings - paper no.6, Brno 23.-24.5.2001, ISBN 80-238-7111-0

Čečrdle, J. (2002) Výpočet vířivého flatru pomocí programového systému MSC.NASTRAN, Journal Czech Aerospace Proceedings, 4/2002, pp.26-30, ISSN 1211-877X

Čečrdle, J. (2002) Vliv poruchy letecké konstrukce na její dynamické chování, Ph.D. thesis, ČVUT Praha, 2002

Čečrdle, J. (2005) Výpočet vířivého a křidélkového flatru křídla s motorem aeroelastického modelu letounu L-610, VZLU Report, V-1839/3210/05

FAR Part 23, Amendment 23-52; Advisory Circular No. 23.629-1A; FAR Part 25, Amendment 25-99; Advisory Circular No. 25.629-1A

MIL-A-8870C(AS); Airplane Strength and Rigidity - Vibration, Flutter and Divergence